



Flue Dust Reactions and Sticking Mechanisms in a Copper Flash Smelting Furnace Waste Heat Boiler: A Sampling Study

Amélia Schmidt¹ · Bradley Martin Guy¹ · Victor Montenegro² · Markus Reuter³ · Alexandros Charitos³ · Michael Stelter¹ · Andreas Richter⁴

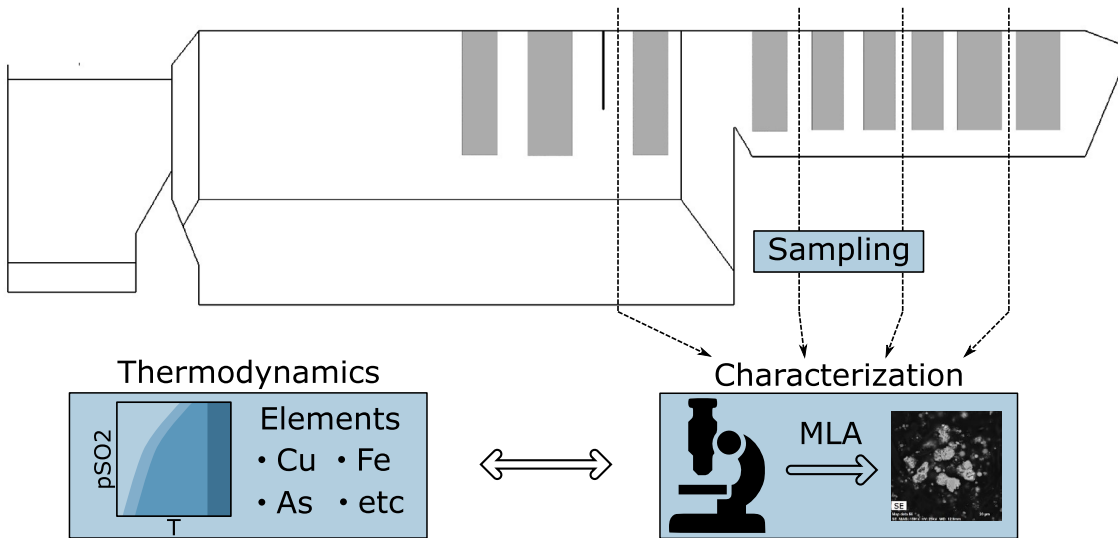
Received: 24 October 2022 / Accepted: 18 April 2023

© The Author(s) 2023

Abstract

The formation of accretion layers within the waste heat boiler is a serious operational concern as it can potentially increase boiler downtime and, hence, limit continuous production. In previous Computational Fluid Dynamics studies, the accretion formation was predicted for an industrial-scale waste heat boiler, using a dust stickiness sub-routine of the model. In this study, a dust sampling campaign was used to validate this stickiness sub-routine. Furthermore, various sticking and reaction mechanisms of flue dust were investigated and compared to thermodynamic predictions. While the results suggest that the sub-routine is valid, the comparison of thermodynamics and species in the samples showed that the chemical reactions of the flue dust did not reach the thermodynamic equilibrium.

Graphical Abstract



Keywords Flash smelting furnace · Waste heat boiler · Flue dust · Accretions · Sampling study · CFD

The contributing editor for this article was Sharif Jahanshahi.

✉ Amélia Schmidt
am.schmidt@aurubis.com

¹ Helmholtz Institute Freiberg for Resource Technology,
Chemnitzer Strasse 40, 09599 Freiberg, Germany

² Aurubis AG, Hovestrasse 50, 20539 Hamburg, Germany

³ Institute for Nonferrous Metallurgy and Purest Materials,
TU Bergakademie, Leipziger Strasse 34, 09599 Freiberg,
Germany

⁴ Professorship for Modeling of Thermochemical Conversion
Processes, TU Bergakademie, Fuchsmühlenweg 9,
09599 Freiberg, Germany

Introduction

Copper is one of the most important metals for achieving a circular economy and resource efficiency [1]. To satisfy the increasing demand of this metal, primary production of copper remains crucial. The Flash Smelting Furnace (FSF) is a widely used technology for copper primary production [1, 2]. Because the FSF necessitates dry and fine concentrate material, approximately 5% of the concentrate input mass is carried over into the downstream waste heat boiler (WHB) and forms flue dust. The flue dust is the cause of various operational challenges, such as accretion formation and blockages, which can limit the boiler availability [3–5]. In addition to mechanical dust formation, dust can also be produced by the chemical condensation of vaporized species, which can result in complex dust compositions and morphologies [6, 7].

Flue dust can either be disposed, treated for the recovery of valuable elements, or recycled into the FSF [6]. The recyclability of flue dust is limited by its content of impurities, such as arsenic, lead, zinc, or bismuth [7, 8]. Hence, important operational goals include the control of various chemical reactions and cooling parameters, as well as flue dust settling dynamics. This might allow for the controlled deposition of flue dust rich in certain metals, simplifying later remediation and recycling [6, 7].

More insight into the behavior of flue dust in the WHB can be obtained by dust sampling or thermodynamic studies. For flue dust sampling, the following procedures have been reported by previous studies:

1. Collection of settled flue dust from the bottom of the radiation or convection section or from the electrostatic precipitator (ESP) [3, 9, 10]. A preliminary study showed that the strong aggregation of the resulting samples complicates the evaluation of particle size distributions (PSD).
2. Collection of flue dust in the form of boiler accretions and deposits [11–13].
3. Removing dust directly from the process gas using a ceramics crucible (only for copper converter) [6, 7].
4. Removing dust directly from the process gas using a vacuum pipe [12] (for Mitsubishi-type smelter in [11]).

Different procedures and different sampling locations can strongly influence flue dust morphology, composition, and mineralogy. Regarding the particle morphology, Chen et al. [3] found that the median particle size decreases along the length of the WHB, using samples from the radiation section, the convection section, the dust settling chamber (DSC), and the ESP obtained by sampling procedure 1. This shows that the coarse particles settled in the

early parts of the off-gas treatment, while small particles are carried over with the process gas, causing a progressively smaller median particle size. The dust particles were found to be irregularly shaped. In contrast, Balladares et al. [9] reported the particles from WHB and ESP to be mainly spherical when sampling with procedure 1. The WHB sample was coarser and had a wider size distribution; the maximum particle size decreased from 79 to 9 μm comparing WHB and ESP. Another study used sampling procedures 1, 2, and 4, showing the resulting differences in particle morphology caused by sampling [12]: When using procedure 1, the samples showed single particles with a diameter up to 50 μm in the radiation section. When using sampling procedure 4, the particles were smaller and aggregated. The authors suggested that these agglomerates not only might have occurred in the gas stream, but might also be caused by the sampling technique.

Regarding the transformations of the main elements, copper, iron, and sulfur, X-ray fluorescence spectrometer (XRF) results showed that the content of copper in the dust decreased slightly from 29.2 wt% to 25.6 wt% comparing WHB to ESP samples, while iron did not show this tendency, with its content varying from 16.6 wt% to 19.0 wt% [3]. Phases containing compositions of Fe_3O_4 (magnetite) and CuSO_4 were the most common of the crystalline phases in the flue dust [3]. This finding was confirmed by Balladares et al. [9], where XRD analysis showed that $\text{CuSO}_4 \cdot 5\text{H}_2\text{O}$ and Fe_3O_4 were the most common phases for WHB and ESP samples, followed by Fe_2O_3 and CuFeO_2 , while, in contrast to [3], the copper content did not vary with the location of the sampling.

Using sampling procedure 4, particles from the radiation section showed a layered structure, with an oxidic copper iron core surrounded by a sulfate layer [12]. In contrast, the samples taken from the accretions in the convection section consisted mainly of copper sulfate.

Regarding the arsenic species, Chen et al. [3] found the arsenic content to increase from 2.5 wt% in the WHB to 4.2 wt% in the ESP. Over 80% of arsenic was found in the form of arsenate, followed by less than 10% As_2O_5 , which increased from the convection section to the ESP. A minor fraction of elemental arsenic was found in the radiation section sample, showing the progressive oxidation of arsenic in the off-gas system. The study by Balladares et al. [9] confirmed the increasing arsenic content, from 0.8 wt% in the WHB to 2.0 wt% in the ESP.

The composition of dust samples obtained by sampling procedure 2 differs from that of dust samples obtained by other sampling procedures. This might be caused by the different physical conditions under which the dust is sampled: While the settled flue dust is located in the colder lower regions of the WHB, dust in the form of accretions can be exposed to higher temperatures, possibly

chemically reacting further with the main gas flow. Additionally, the dust is more likely to have been sticky before the sampling, creating a bias towards dust compositions with a low melting point. Fernández-Caliani et al. [13] investigated accretion samples from the entrance area of the WHB. Two types of accretions were found, where type I was more prevalent. Type I consisted of approx 50 wt% Fe_3O_4 , 25 wt% CuFeO_2 (delafoseite), and 20 wt% glass consisting of silica. The remaining phases were Cu_2O (cuprite) and metallic copper. Type II consisted of up to 70 wt% of Fe_3O_4 , with 10 wt% to 20 wt% Fe_2SiO_4 (fayalite), up to 15 wt% Si-glass and a minor amount of Cu_2S (chalcoelite). Markova et al. [14] used samples from the entrance of the WHB, the radiation section, and the convection section. The process conditions in the WHB were not given. It was found that the sulfate content increased along the WHB until max. 97%. This sulfate can mainly be found in copper sulfate, whereas iron sulfate is only a minor component. Tests showed that the stability of the following sulfates decreased as follows: $\text{PbSO}_4 > \text{ZnSO}_4 > \text{CuSO}_4 > \text{FeSO}_4$. The main components of the samples were found to be Fe_3O_4 and CuSO_4 . Miettinen [12] found accretions, which were “glued” by former liquid copper arsenic oxide and by copper sulfate in the radiation section, while accretions in the convection section were glued by only copper sulfate.

When using thermodynamics to investigate the limit of the chemical reactions of dust, it is important to know that the thermodynamic equilibrium is not always reached in the WHB, especially at lower temperatures [4]. For the WHB gas uptake, Swinbourne et al. [4] predicted accretions to consist of PbSO_4 , Fe_2O_3 and ferrites. However, ferrites are not commonly reported from sampling studies. Illiev et al. [5] found that FeS was more likely to convert to Fe_3O_4 and Fe_2O_3 than to iron sulfate over the entire investigated temperature range from 1250 °C to 350 °C. At the same temperature range, CuFeS_2 (chalcopyrite) is predicted to convert to copper spinel, while copper sulfides would more likely react to copper oxide and metallic copper, thereby increasing the likelihood to combine as $\text{Cu}_2\text{O} \cdot \text{Fe}_2\text{O}_3$ with decreasing temperatures.

In the radiation section, Swinbourne et al. [4] predicted accretions based on Fe_3O_4 , copper, and lead sulfides. PbS was considered to be more sticky than PbSO_4 . When oxygen was added, the thermodynamic calculations showed that the sulfide species reacted to oxides and sulfates, reducing the dust stickiness. At 800 °C, lesser amounts of CuSO_4 were found than in comparable dust samples from the radiation section. A minor share of arsenate was predicted. Illiev et al. [5] found that the iron oxidation was favored in the radiation section compared to the sulfatization, which could occur only at temperatures below 700 °C.

For the convection section, Swinbourne et al. [4] predicted the following composition of flue dust regarding the

most prevalent species: 25 wt% $\text{Fe}_2(\text{SO}_4)_3$, 25 wt% PbSO_4 , 20 wt% CuSO_4 , 15 wt% ZnSO_4 , and 5 wt% $\text{Cu}_3(\text{AsO}_4)_2$. The study by Illiev et al. [5] supports this finding, predicting that the formation of cupric and ferrous sulfates should occur from a thermodynamic point of view. Samuelsson et al. [15] found that volatile components in the process gas would condense as sulfides in the case of low oxygen content, and as oxides and sulfates in case the oxygen partial pressure was sufficient. When oxides and sulfates are formed, the solidus temperature is increased compared to sulfides, hence reducing the particle stickiness.

Swinbourne et al. [4] predicted that arsenic condenses only if the process gas has a high oxygen content. Samuelsson et al. [15] found that the initial As_2S_3 oxidizes to As_2O_3 and further to As_2O_5 depending on the available oxygen.

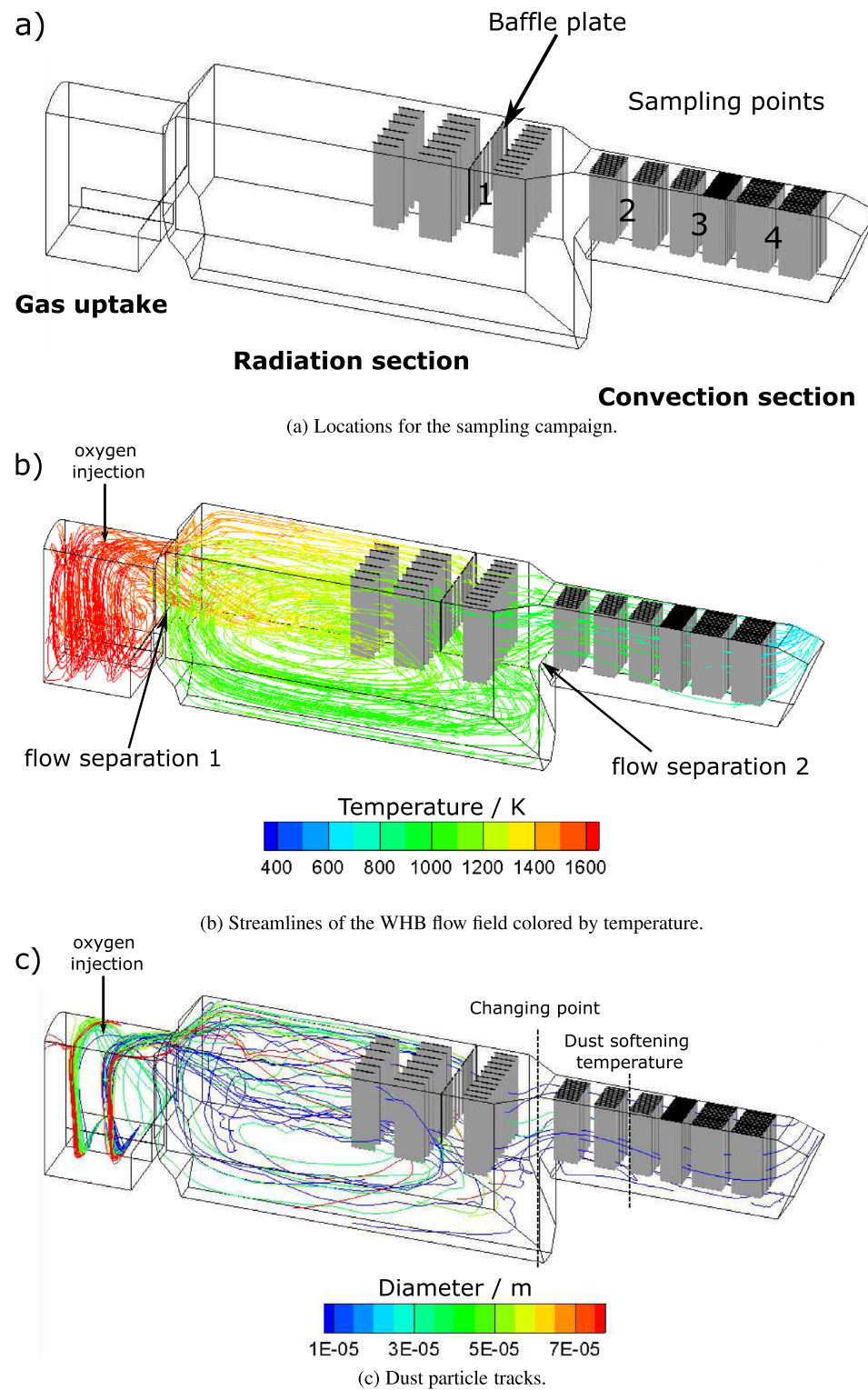
In previous studies, the accretion formation was predicted with a Computational Fluid Dynamics (CFD) model [16]. As a sticking criterion for the dust particles, a dust softening temperature of 700 °C was used, a figure estimated by industrial experience. Thereby, dust is considered sticky above this temperature, because it has either liquid components or other kind of components or structures, such as fast crystallizing species, which can bind together and create accretions. In the literature, it is mentioned that the dust softening temperature correlates to the sintering temperature of the sulfated particles without specifying an exact value [17]. This study aims to validate the dust softening temperature by a sampling study, as well as to extend the knowledge on the mechanisms behind dust stickiness. Therefore, isokinetically sampled dust was collected from four locations along the length of the WHB, applying an improved sampling and preparation procedure.

Sampling Locations, Sampling and Preparation

The dust samples were retrieved from the Aurubis AG WHB at Hamburg primary smelter, into which, as a common practice, additional oxygen was injected into the gas uptake. Flue dust was sampled behind the baffle plate in the radiation section and on three sampling points along the length of the convection section, as sampling before the baffle plate is not possible due to the high temperatures over 1000 °C. The sampling points are depicted in Fig. 1a.

- Sampling point 1: Behind the baffle plate in the radiation section.
- Sampling point 2: At the beginning of the convection section.
- Sampling point 3: In the middle of the convection section.
- Sampling point 4: At the end of the convection section.

Fig. 1 Geometry, gas flow, and particle settling in the WHB



The accessibility to the WHB is limited due to its in-housing, making sampling only possible at a few locations. For this study, sampling was conducted at a medium height, so that representative samples can be retrieved from the main gas flow. As sampling before the baffle plate was not possible,

the four sampling locations were chosen to be evenly spaced in the remaining part of the radiation section and in the convection section. The sampling probe shown in Fig. 2 was inserted into the center of the WHB, from where the dust

was removed directly from the gas stream for a sampling time of 60 minutes and collected in a heated quartz filter.

Upon completion of the sampling, the filter was placed in an airtight container with silica gel to prevent the flue dust from reacting with ambient humidity. This approach ensured that 75% of the copper sulfates remained in their original, water-free form. For comparison, electrostatic precipitator dust (ESP) sampled in a preliminary study, in which the airtight container was not used, contained less than 5% water-free copper sulfates. In the preparation step, the flue dust was removed carefully from the filter material and divided into representative sample fractions using a sample divider. For the electron microscope analysis, and for each sampling location, a split aliquot of the material was embedded in epoxy resin, cut into vertical slices and then embedded in resin again to account for density settling. The samples were ground on diamond grinding disks with ethylene glycol and polished with a suspension of micro-diamonds and ethylene glycol. This procedure is water free.

Microscopy Methods

Automated mineralogical analyses were conducted on 30-mm-diameter polished epoxy mounts (transverse cut) from each flue dust sample using a Mineral Liberation Analyzer (MLA). The ThermoFisher Scientific MLA 650F was equipped with two XFlash Bruker detectors (5030). The data outputs included modal mineralogy (area %), particle size distribution, and roundness. Roundness was calculated using the expressions in QEMSCAN given in [18]. The following MLA parameters were used:

- kV: 25
- Specimen current: 10 nA
- Working distance: 13 mm
- Spot Size: 5.7

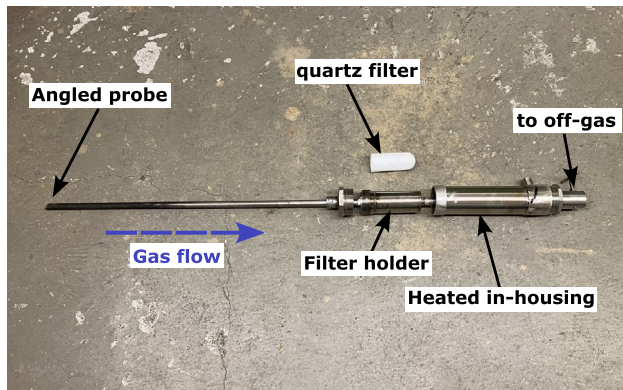


Fig. 2 Sampling probe

- X-Ray calibration: copper
- MLA Measurement program: GXMAP
- BSE calibration: copper (250 BSE)
- Frame size (HFW): 200 micron
- Dwell time/resolution: 8/800
- X-ray step/spacing size: 2 micron
- X-ray spectrum count > 2500
- Average particle count/sample: 220k

Parameters 1 to 5 represent the standard SEM conditions used for the MLA measurements. Parameters 6 to 12 represent the MLA measurement settings. These settings were conducted at high magnification (200 micron frame size) and dense X-ray spacings (2 micron) using the GXMAP program (grid-based X-ray mapping) to account for the fine-grained nature of the flue dust material. Element maps were collected on the ThermoFisher MLA 650F using the two X-flash Bruker detectors (5030) and the Bruker Esprit mapping software.

Results

CFD Calculations: Dust Separation in the WHB

A detailed description of the numerical model can be found in [16]. Figure 1 shows the most important findings correlating to the present sampling study. Figure 1a depicts the WHB geometry, consisting of three main compartments: the gas uptake, the radiation section, and the convection section. Three rows of cooling screens and a baffle plate are located in the second half of the radiation section, and six rows of boiler tubes are located in the convection section. The streamlines of the process gas flow are given in Fig. 1b, indicating the complex flow field in the WHB. They are colored by gas temperature. When the hot process gas enters the radiation section, the largest fraction of the flow will bypass the radiation section along the roof and enter the convection section. However, a smaller share recirculates in the lower half, leading to a flow separation at the end of the gas uptake. The flow changes its direction sharply, which leads to an area with large temperature differences. These flow separations facilitate the removal of larger particles from the main flow. When entering the convection section, another flow separation occurs due to the sharp edge at the convection section entrance, creating a dead zone in the lower third of this section.

These flow separations result in the dust particle tracks shown in Fig. 1c. Sticky particles are especially prone to accretion formation in the beginning of the radiation and convection section, where the main flow is directly aimed at the WHB walls and the boiler tubes. With regard to the

sampling points, this results in more profound changes in dust size and mineralogy between point 1 and 2 (changing point) and 2 and 3 (dust softening temperature).

Studies on Dust Stickiness

Estimation of Dust Softening Temperature

The isokinetic flue dust sampling leads to aggregate formation of the sampled material if the dust particles are sticky. While aggregating, two particle characteristics change: i) the average particle diameter increases, as primary particles are glued together to form larger aggregates, and ii) the particle shape factor decreases, since aggregates can have varying shapes and are hence less circular than the primary particles, which were found to be mostly spherical in shape.

While conducting the flue dust sampling for sampling point 2, aggregated material was observed within the sample. Consequently, it was not possible to determine the dust softening temperature based on particle size distribution according to the first particle characteristics. Instead, the shape factor was used as a criterion to determine the accretion formation. Furthermore, it was considered that the particle collisions are similar for each sample since the majority of the collisions are caused by the sampling technique, i.e., the vacuum pipe. Primary particles in this system are mainly spherical and have a roundness close to 1.0. Figure 3 shows the shape factor distribution for each sampling point depending on the particle or aggregate

size. Sampling points 1 and 2 show a very scattered shape factor distribution at sampling temperatures of 725 °C and 720 °C, respectively. The particle size distribution is biased towards larger, more aggregated particles. Sampling point 3 and 4 have a similar, more narrow distribution of shape factors at sampling temperatures of 600 °C and 560 °C. The focus lies on spherical, smaller particles at a roundness of 0.5 and a size of approximately 3 μm to 10 μm. This size group is close to the one described for ESP dust samples [9].

This finding can also be confirmed qualitatively when comparing larger aggregates sampled before and after cooling below the dust softening temperature, as depicted in Fig. 4. Figure 4a shows an aggregate, which was sampled at sampling point 2 (720 °C). It has a compact, strongly fused structure, in which the primary particles are not clearly visible. In contrast, figure 4b shows a loosely-structured aggregate with clearly visible primary particles, which was sampled at sampling point 4 (560 °C). This structure was found to be representative for aggregates sampled below the dust softening temperature.

Based on the changes in size, shape, and structure of the aggregates, it can then be concluded that the dust softening temperature must be in the range of 600 °C to 720 °C, between sampling points 2 and 3. While this temperature range comprises the dust softening temperature, it is not possible to derive a distinct softening temperature from it. However, the temperature range supports the selection of the sticking criterion derived from industrial experience, which

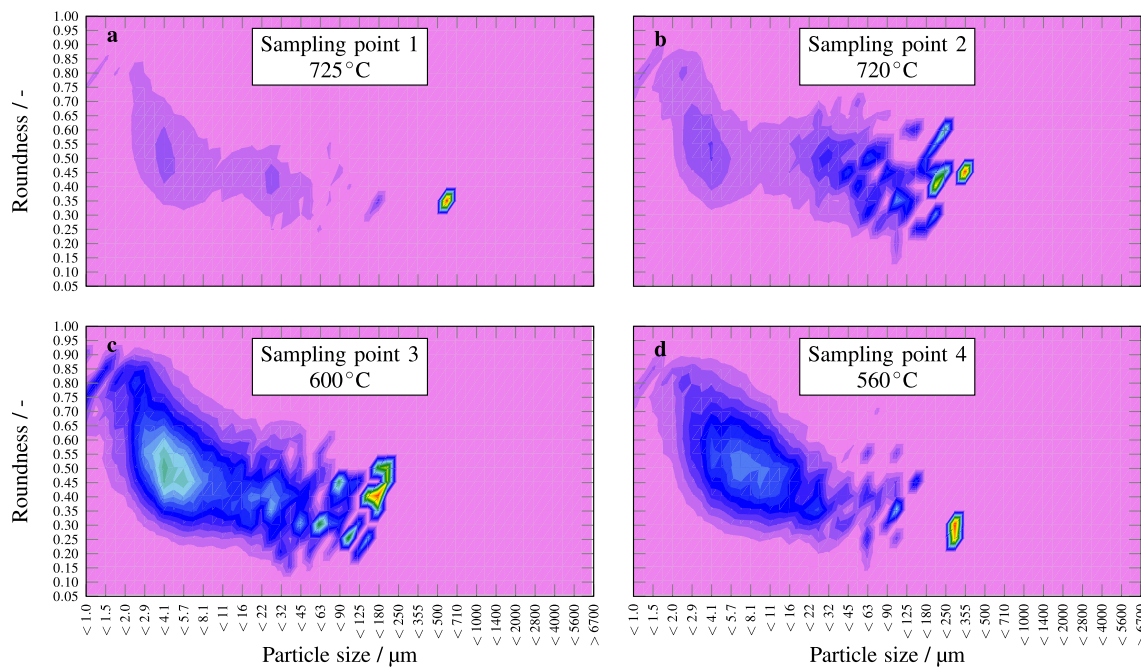


Fig. 3 Particle shape factor at four sampling points

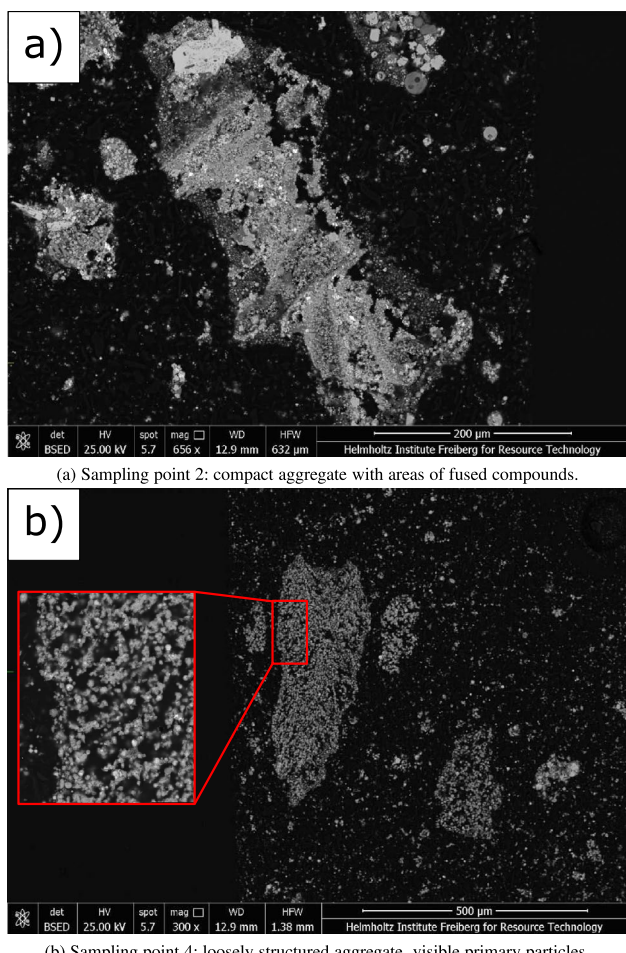


Fig. 4 BSE images: Comparison of large aggregates from sampling point 2 and 4

considers dust to be sticky above a temperature of 700 °C, suggesting that the dust sticking criterion used in previous CFD models is acceptable.

Mechanisms for Aggregate Formation

Figure 5 shows the different mechanisms of aggregate formation.

Table 1 summarizes the sticking mechanisms.

Fused Cu-Fe oxides Fig. 5a to 5c shows the Back-Scattered Electron (BSE) images and element maps of aggregates consisting of fused oxidic Cu-Fe primary particles of spherical shape. This direct fusion of primary particles, indicating a mechanism of agglomeration without another species acting as glue, was not commonly observed in the samples. The primary particles are most likely former concentrate carried over from the FSF. Fusion of Cu-Fe oxides can only occur at high temperatures, explaining why they were only found at sampling point 1. In this study, the fused aggregates consisted of maximum three primary particles. However, since only small aggregates can follow the

gas flow until behind the baffle plate, the sampling procedure might be biased towards smaller fused Cu-Fe oxide aggregates. However, this does not preclude the formation for larger accretions, since only small aggregates can follow the gas flow into the baffle plate. Thus, the sampling procedure might be biased towards smaller fused Cu-Fe oxide aggregates.

Cu-As oxides as glue Fig. 5d to 5f shows BSE images and element maps of the second mechanism, in which primary particles are connected by low-melting Cu-As oxides. This mechanism was found at sampling points 1 and 2. The observed removal of arsenic from the gas flow and the thermodynamic explanation are given in Section “Arsenic”.

Cu sulfates as glue Copper sulfate as a means of aggregate formation above the dust softening temperature is depicted in Fig. 5g to 5i. The copper sulfate shows a high crystallinity, which can be explained by the high crystal-growth rate at higher temperatures. Copper sulfate does not always occur as single primary particles, but is more commonly observed as the binding agent between primary particles. Cu-As oxides occur as a second sticking mechanism and were frequently observed within the same aggregates. When the temperature is below the dust softening temperature, the sulfate shows reduced crystallinity with a looser structure, suggesting weaker bonds between the primary particles (see Fig. 5j to 5l). This might lead to less and brittle accretions towards the end of the convection section, as is observed in industrial application, when the accretions are removed during WHB maintenance. The shrinking core mechanism of dust sulfatization is clearly visible in Fig. 5l, since each oxidic core is surrounded by a thin copper sulfate rim. Although it was found to be the most important dust sticking mechanism within the sampled area, this finding does not extrapolate to the warmest compartments of the WHB. Instead, it must be noted that accretions with sulfates will decompose above the sulfate stability temperature of approximately 800 °C. Hence, sulfatization cannot be the primary means of accretion formation in the gas uptake and the entrance of the radiation section.

Dust Mineralogy

Dust Composition: MLA Analysis and Thermodynamic Considerations

Table 2 summarizes the flue dust composition as determined by MLA. The two main phases are copper sulfate and Cu-bearing iron oxides (5–10% Cu). While the area fraction of copper sulfate increases from 46% at sampling point 2 to 80% to sampling point 4, the iron oxide share is increasing from sampling point 1 to sampling point 2, before decreasing in accordance with the increasing copper sulfate share. Silicates and Cu-Fe oxides decrease continuously from a share of 14% and 16% to 6% and 4%, respectively, while gypsum shows a similar behavior as the iron oxides.

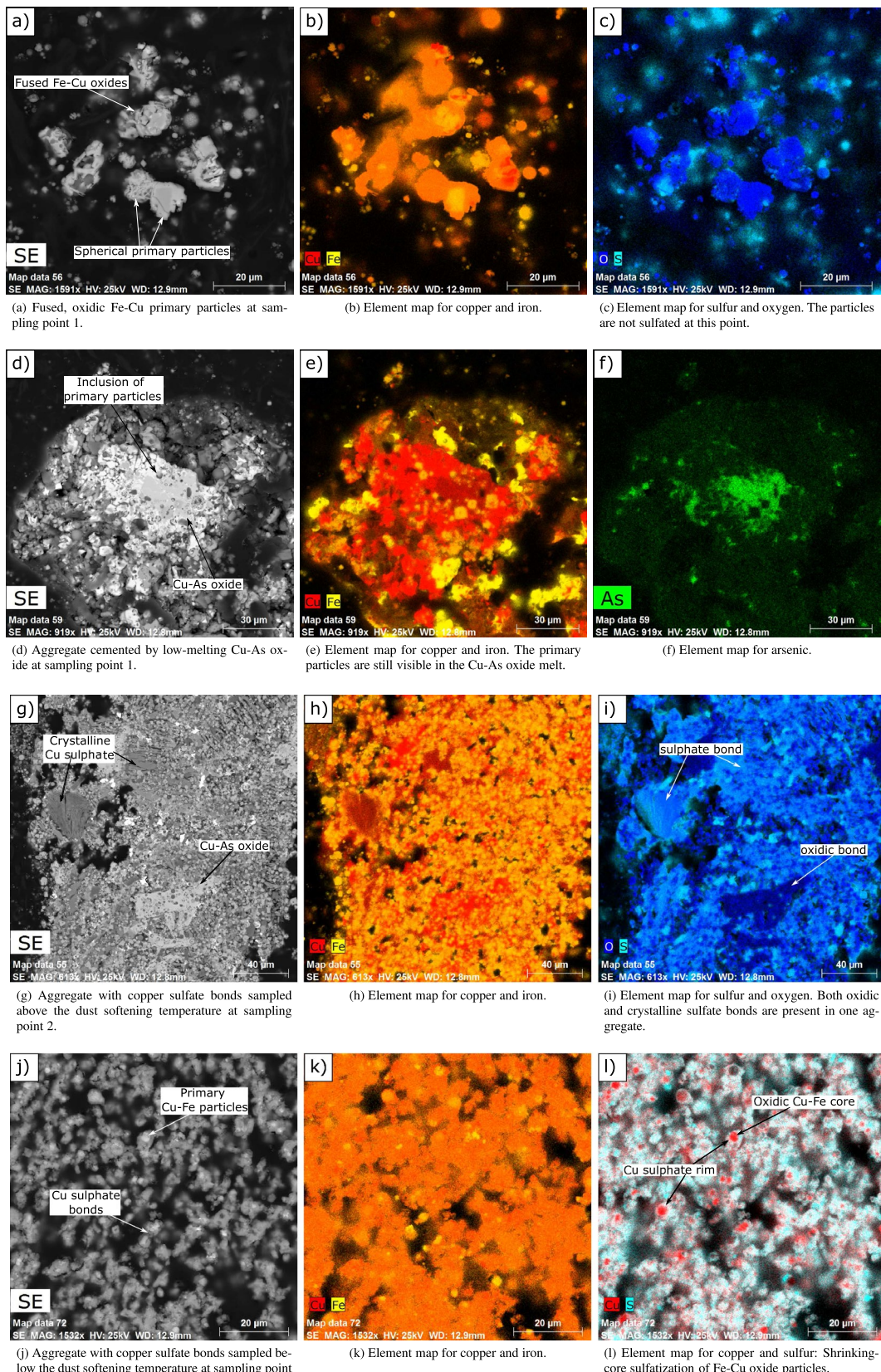


Fig. 5 Examples for the sticking mechanisms: Fusing of Fe-Cu oxides (5a to 5c), low-melting Cu-As oxide (5d to 5f) and CuSO_4 formation above and below the dust softening temperature (5g to 5i vs. 5j to 5l)

Table 1 Occurrence of the three sticking mechanisms in the samples				
Sticking mechanism	Sampling point 1 725 °C	Sampling point 2 720 °C	Sampling point 3 600 °C	Sampling point 4 560 °C
Fused Cu-Fe oxides	X			
Cu-As oxides	X	X		
Cu sulfates	X	X	X	X

Table 3 summarizes the chemical alterations of the most common copper concentrate minerals along the length of the WHB. Since these elements are present in the concentrate, they might occur in the flue dust and carry-over material. Hence, they are shown for a complete overview. However, because some elements like Mn and Mo can only be present in very small amounts, their influence on the accretion formation is probably negligibly small. The calculations were performed in HSC Chemistry 10 with the respective metal-oxygen-sulfur systems at a constant oxygen fraction of 5% (see [5]). Comparing to the dust composition in 2, the following species were reported in the dust samples: arsenic oxide (unknown oxidation state), CaSO₄, Cu₂O, CuO, CuSO₄, Fe₂O₃, Fe₂(SO₄)₃, PbSO₄, SiO₂ (as silicates). Based on these thermodynamic calculations, multiple species might form accretions in the gas uptake and radiation section entrance, such as Cu₂O, MgSO₄, PbO or PbSO₄. However, this finding cannot be validated based on this sampling study since no samples were taken from the gas uptake or the radiation section entrance.

The different oxidation and sulfatization degrees of copper and iron were present in the samples and are further investigated in Section “Copper and Iron Minerals: Oxidation and

Sulfatization”. The only reported species which is liquid within the sampled area and, hence, might be sticky, is arsenic oxide. The behavior of arsenic is investigated in Section “Arsenic”.

Copper and Iron Minerals: Oxidation and Sulfatization

Figure 6a shows the presence of Cu₂O and CuO in the samples.

As shown in the thermodynamic calculations in Table 2, Cu₂O in the flue dust is oxidized to CuO while moving through the WHB. However, since Cu₂O was still found at the end of the convection section, this oxidation does not reach completion. In accordance to this finding, iron is oxidized from Fe₃O₄ over γ-Fe₂O₃ (maghemite) to Fe₃O₄ (hematite) as shown in Fig. 6b. Again, this conversion does not reach thermodynamic equilibrium. Figure 6c shows the fraction of copper and iron sulfates as determined by MLA. At sampling points 1 and 2, the area fraction of copper sulfates remains constant at approximately 50%. Until this point, the dust temperature is above the dust softening temperature, most likely resulting in accretion formation or settling of aggregates, binding the sulfated dust. From sampling point 3 on, the dust is less sticky, and hence, sulfates are more likely to be sampled, although the rate of sulfatization decreases with temperature. This explains the gradual increase of sulfates to up to 80% at sampling point 4. The same behavior is observable for iron sulfates, despite at a lower level of maximum 1.5%. A comparison of the Gibbs free energy for the copper and iron sulfatization shows that the copper sulfatization remains the thermodynamically favored sulfatization reaction throughout the entire WHB temperature range. Hence, iron sulfatization can only be a local phenomenon, where copper is not available as a reaction partner.

Table 2 Overview over sample compositions as determined by MLA (Area %) (rounded values)

Species	Sampling point 1 725 °C	Sampling point 2 720 °C	Sampling point 3 600 °C	Sampling point 4 560 °C
Copper sulfates	47.0	46.0	62.1	79.6
Iron sulfates	0.3	0.1	1.3	1.4
Gypsum/anhydrite	2.1	2.6	1.0	1.0
Other sulfates	0.1	0.1	0.1	0.0
Total sulfates	49.5	48.8	64.4	82.0
Iron oxides (with Cu)	19.6	25.3	20.1	8.2
Cu-Fe oxides	16.1	13.6	6.9	3.59
Copper oxides	0.1	0.2	0.00	0.00
Cu-As oxide	0.3	1.1	0.0	0.0
Total oxides	36.1	40.1	27.1	11.8
Silicates	14.1	10.6	8.4	6.0
Sulfides	0.0	0.1	0.0	0.0
Other	0.4	0.4	0.1	0.2
Total	100.0	100.0	100.0	100.0

Bold values indicate sum of the species above

Table 3 Thermodynamically-stable species in each WHB compartment and their melting points or boiling points (BP) at $p_{O_2} = 5\%$ (see [5]) (calculated in HSC Chemistry 10)

Element	Gas Uptake	Radiation section	Convection section
	1350 °C - 1000 °C	1000 °C - 700 °C	700 °C - 350 °C
Al	Al_2O_3 2054 °C	$Al_2O_3 \rightarrow Al_2(SO_4)_3$ 2054 °C → Decomposition	$Al_2(SO_4)_3$ Decomposition
As	$As_2O_3(g)$ 465 °C (BP)	$As_2O_3(g) \rightarrow As_2O_5^*$ 465 °C (BP) → 730 °C	$As_2O_5^*$ 730 °C
Ca	$CaSO_4^*$ 1460 °C	$CaSO_4^*$ 1460 °C	$CaSO_4^*$ 1460 °C
Cd	$CdO \rightarrow CdSO_4$ 1556 °C (BP) → 1000 °C	$CdSO_4$ 1000 °C	$CdSO_4$ 1000 °C
Cu	$Cu_2O^* \rightarrow CuO^*$ 1235 °C → 1446 °C	$CuO^* \rightarrow CuO \cdot CuSO_4 \rightarrow CuSO_4^*$ 1446 °C → Decomposition	$CuSO_4^*$ Decomposition
Fe	$Fe_2O_3^*$ 1565 °C	$Fe_2O_3^* \rightarrow Fe_2(SO_4)_3^*$ 1565 °C → 1178 °C	$Fe_2(SO_4)_3^*$ 1178 °C
Mg	$MgO \rightarrow MgSO_4$ 2832 °C → 1130 °C	$MgSO_4$ 1130 °C	$MgSO_4$ 1130 °C
Mn	Mn_2O_3 1347 °C	$Mn_2O_3 \rightarrow MnSO_4$ 1347 °C → Decomposition	$MnSO_4 \rightarrow Mn_2(SO_4)_3$ Decomposition
Mo	MoO_3 1150 °C (BP)	MoO_3 802 °C	MoO_3 802 °C
Pb	$PbO^* \rightarrow PbO \cdot PbSO_4 \rightarrow PbSO_4^*$ 887 °C → 970 °C	$PbSO_4^*$ 970 °C	$PbSO_4^*$ 970 °C
Si	SiO_2^* 1713 °C → 1425 °C	SiO_2^* 1425 °C	SiO_2^* 1425 °C
Zn	ZnO 1975 °C	$ZnO \rightarrow ZnSO_4$ 1975 °C → 742 °C	$ZnSO_4$ 742 °C

* species were found in sampling study

bold species are liquid

Arsenic

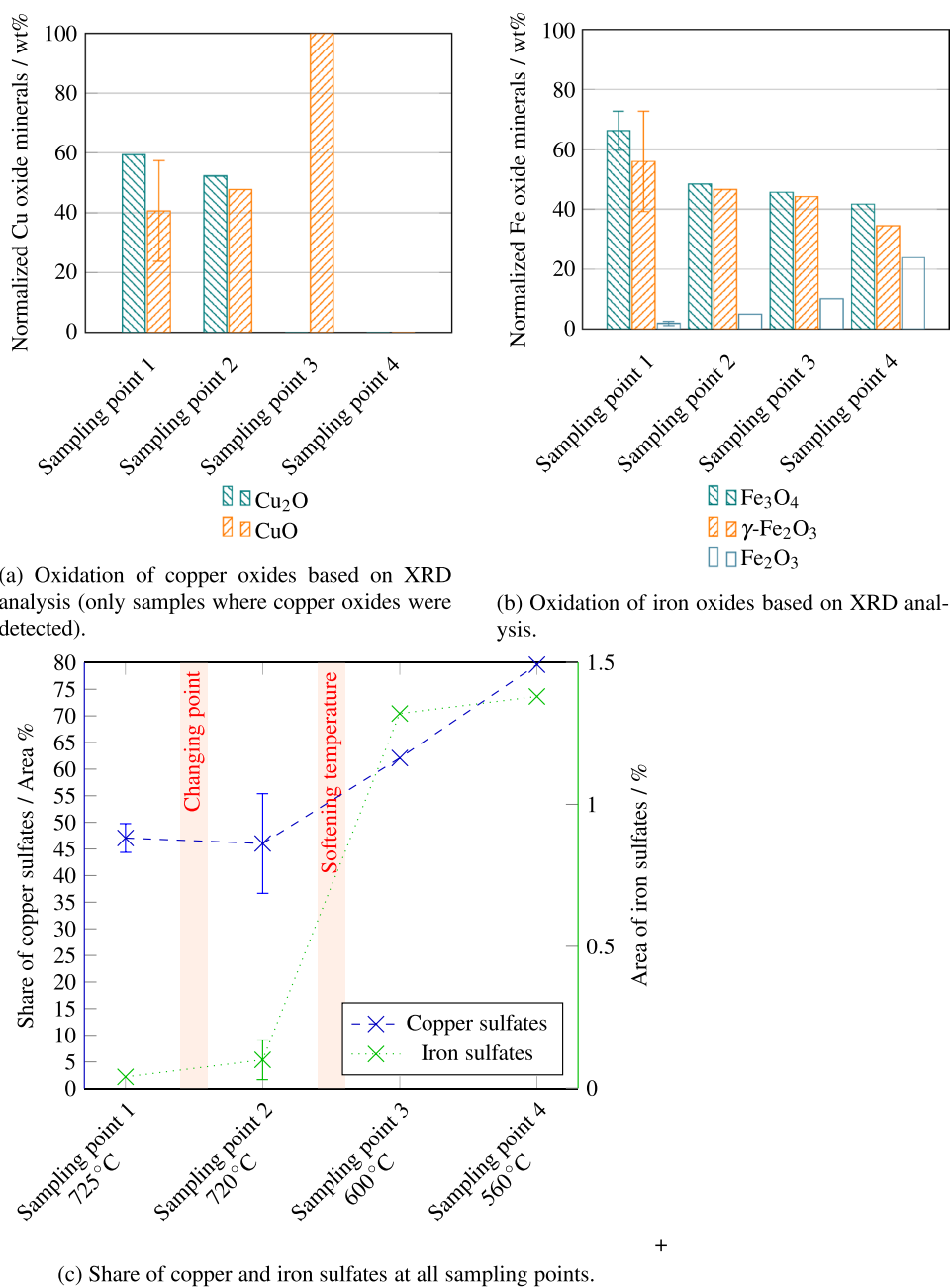
In the sampled flue dust, arsenic occurs predominantly in the form of copper arsenic oxides, although an average of 0.01% was detected in the form of arsenic sulfate at sampling point 1. This value can just serve as an indication for the scarcity of arsenic sulfate, since its proportion is too small for a reliable determination using one sample per sampling point. Figure 7 shows the area fraction of Cu-As oxides for all sampling locations. From sampling point 1 to sampling point 2, the Cu-As oxide mass fraction, as indicated by the percentage area, increases from 0.3 % to over 1.0 %. At these points, the local temperature is in the range of the melting point of As_2O_5 of 730 °C, making the progressive condensation of a liquid arsenic phase possible (see Table 3). The oxidation from As_2O_3 to As_2O_5 is caused by the injection of additional oxygen in the gas uptake. As described in Section “Mechanisms for Aggregate Formation”, a liquid copper arsenic phase can act as a cement for Cu-Fe oxide primary particles. This might explain the sudden decrease

in Cu-As oxides at sampling points 3 and 4, below the dust softening temperature: as soon as the liquid arsenic phase forms, it will either form larger aggregates or form accretions. In this way, it is removed from the gas stream and from the sampled locations. This finding should be supported by additional sampling from accretions and settled flue dust, in order to investigate the low arsenic mass fractions in a statistically more robust fashion.

Conclusions

This study investigated the changes in mineralogy of flue dust along the length of the WHB by means of a dust sampling study on an industrial-scale WHB during operation. An improved sampling technique was applied to achieve sampling directly from the gas stream at four sampling points, one at the end of the radiation section and three in the convection section. After a water-free sample preparation, it was possible to investigate the dust reaction and

Fig. 6 Oxidation and sulfatization of copper and iron



sticking mechanisms. The samples showed a reduced roundness shape factor between 720 °C and 600 °C, which indicates weaker aggregation. This suggests that the dust softening temperature of 700 °C could be used as a sticking criterion for the sub-routine of previous CFD models. Based on the evidence of morphology and composition, three dust sticking mechanisms could be postulated: (i) direct fusion of Cu-Fe oxides and gluing of primary

particles by (ii) liquid Cu-As oxides or (iii) copper sulfates. The oxidation and sulfatization degrees of copper, iron, and arsenic were compared to thermodynamically stable species in each WHB compartment. While different oxidation and sulfatization degrees of copper and iron were found in the samples, the extent of conversion indicated that thermodynamic equilibrium was not reached.

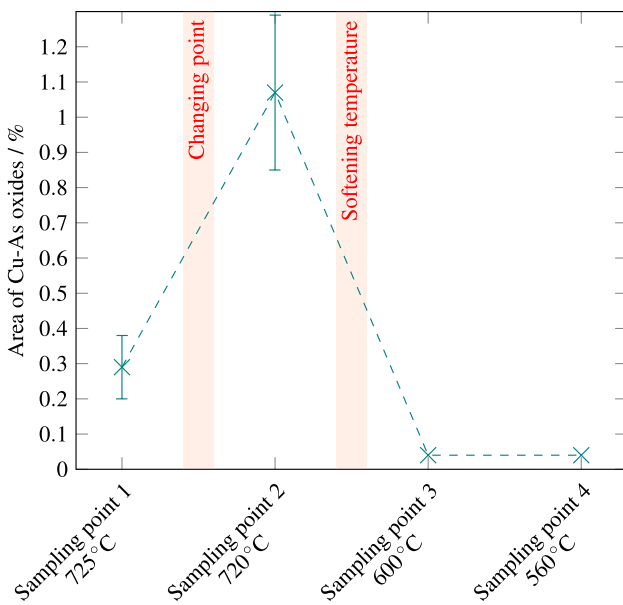


Fig. 7 Mass fraction of Cu-As-oxides per sampling point

Acknowledgements The authors are grateful for the computing time granted on the computer cluster at the Faculty of Mathematics and Computer Science, Technische Universität Bergakademie Freiberg, operated by the computing center (URZ) and funded by the Deutsche Forschungsgemeinschaft (DFG) under DFG grant number 397252409. We thank Stefan Winkler, Daniel Peise, Florian Pfeifer from Aurubis AG and Gottfried Steudtner for their support with the sampling campaign. Roland Würkert from Helmholtz Institute Freiberg for Resource Technology is thanked for sample preparation. Robert Möckel and Doreen Ebert are thanked for the XRD analysis.

Funding Open Access funding enabled and organized by Projekt DEAL.

Conflict of interest The authors declare that they have no conflict of interest.

Open Access This article is licensed under a Creative Commons Attribution 4.0 International License, which permits use, sharing, adaptation, distribution and reproduction in any medium or format, as long as you give appropriate credit to the original author(s) and the source, provide a link to the Creative Commons licence, and indicate if changes were made. The images or other third party material in this article are included in the article's Creative Commons licence, unless indicated otherwise in a credit line to the material. If material is not included in the article's Creative Commons licence and your intended use is not permitted by statutory regulation or exceeds the permitted use, you will need to obtain permission directly from the copyright holder. To view a copy of this licence, visit <http://creativecommons.org/licenses/by/4.0/>.

1. Reuter M, Kojo I (2014) A key enabler of resource efficiency. *World Metall-Erzmetall* 67:46–53
2. Taskinen P, Jokilaakso A (2021) Reaction sequences in flash smelting and converting furnaces: an in-depth view. *Metall Mater Trans B* 52B:3524–3542
3. Chen Y, Zhao Z, Taskinen P, Liang Y, Ouyang H, Peng B, Jokilaakso A, Zhou S, Chen T, Peng N, Liu H (2020) Characterization of copper smelting flue dusts from a bottom-blowing bath smelting furnace and a flash smelting furnace. *Metall Mater Trans B* 51B:2596–2608
4. Swinbourne DR, Simak E, Yazawa A (2002) Accretion and dust formation in copper smelting-thermodynamic considerations. *Sulfide Smelt* 2002:247–259
5. Illiev P, Stefanova V, Shentov D, Lucheva B (2016) Thermodynamic analysis of the sulphatization processes taking place in a dust-gas flow from flash smelting furnace. *J Chem Technol Metall* 51:335–340
6. Samuelsson C, Björkman B (1998) Dust forming mechanisms in the gas cleaning system after the copper converting process:(I). Sampling and characterisation. *Scand J Metall* 27:54–63
7. Björkman B, Eriksson J, Nedor L, Samuelsson C (1996) Waste reduction through process optimization and development. *JOM* 48:45–49
8. Montenegro V, Sano H, Fujisawa T (2008) Revisiting the structure of martensite in iron-carbon steels. *Mater Trans* 49(9):2112–2118
9. Balladares E, Kelm U, Helle S, Parra R, Araneda E (2014) Chemical-mineralogical characterization of copper smelting flue dust. *DYNA* 81(186):11–18
10. Okanigbe DO, Popoola API, Adeleke AA (2017) Characterization of copper smelter dust for copper recovery. *Procedia Manuf* 7:121–126
11. Evans JP, Mackey PJ, Scott JD (1991) Smelter process gas handling and treatment. Springer, New York, pp 135–142
12. Miettinen E (2008) Thermal conductivity and characteristics of copper flash smelting flue dust accretions. PhD Thesis, Helsinki, Finland
13. Fernández-Caliani JC, Moreno-Ventas I, Bacedoni M, Ríos G (2017) Mineral chemistry and phase equilibrium constraints on the origin of accretions formed during copper flash smelting. *Miner Metall Process* 34(1):36–43
14. Markova T, Boyanov B, Prionkov S, Shopov N (2000) *J Mining Metall* 26:195–208
15. Samuelsson C, Björkman B (1998) Cleaning system after the copper converting process. *Scand J Metall* 27:64–72
16. Schmidt A, Montenegro V, Reuter M, Charitos A, Stelter M, Richter A (2022) CFD study on the physical behavior of flue dust in an industrial-scale copper waste heat boiler. *Metall Mater Trans B* 53B:537–547
17. Ranki-Kipilnen T, Peuraniemi EJ, Mäkinen M (2002) Sulphation of cuprous oxide in SO₂-rich atmospheres. *Sulfide Smelting* 2002:261–271
18. Little L (2016) The development and demonstration of a practical methodology for fine particle shape characterisation in minerals processing. PhD Thesis, University of Cape Town

Publisher's Note Springer Nature remains neutral with regard to jurisdictional claims in published maps and institutional affiliations.

References

1. Reuter M, Kojo I (2014) A key enabler of resource efficiency. *World Metall-Erzmetall* 67:46–53